Supplement of Atmos. Chem. Phys., 14, 7213–7231, 2014
http://www.atmos-chem-phys.net/14/7213/2014/
doi:10.5194/acp-14-7213-2014-supplement

Atmospheric Chemistry and Physics Open Access

Supplement of

Radiative signature of absorbing aerosol over the eastern Mediterranean basin

A. K. Mishra et al.

Correspondence to: Y. Rudich (yinon.rudich@weizmann.ac.il) and I. Koren (ilan.koren@weizmann.ac.il)

Supplement of Atmos. Chem. Phys., 14, 7213–7231, 2014
http://www.atmos-chem-phys.net/14/7213/2014/
doi:10.5194/acp-14-7213-2014-supplement

Atmospheric Chemistry and Physics Open Access

Supplement of

Radiative signature of absorbing aerosol over the eastern Mediterranean basin

A. K. Mishra et al.

Correspondence to: Y. Rudich (yinon.rudich@weizmann.ac.il) and I. Koren (ilan.koren@weizmann.ac.il)

Supplementary Materials for the Manuscript "Radiative Signature of Absorbing Aerosol over the Eastern Mediterranean Basin"

Amit Kumar Mishra[1], Klaus Klingmueller[2], Erick Fredj[1], Jos Lelieveld[3], Yinon Rudich[1,*], Ilan Koren[1,*]

[1]Department of Earth and Planetary Sciences, Weizmann Institute of Science, Rehovot 76100, Israel

[2] The Cyprus Institute, PO Box 27456, 1645 Nicosia, Cyprus

[3] Max Planck Institute for Chemistry, PO Box 3060, 55020 Mainz, Germany

Table S1 Averaged Optical properties of (level 2) of Mediterranean AERONET sites used in this study. 'N' represents the number of level 2 observation days used in analyses (entire data). The subscripts of parameters name show wavelength in nm. Period (L2)* shows the time span of available AERONET level 2 data for respective sites. More details on seasonal availability of level 2 data for each site can be found in Mallet et al. (2013).

Site Name	N	$AAE_{440\text{-}870}$	$EAE_{440\text{-}870}$	AOD_{440}	SSA_{440}	$AAOD_{440}$	$ASYP_{440}$	Period (L2)*
Pollution Dominated Sites								
Athens	708	1.35±0.42	1.39±0.41	0.23±0.12	0.91±0.03	0.04±0.01	0.70±0.02	2008-2012
Avignon	1816	1.23±0.46	1.47±0.32	0.20±0.13	0.91±0.03	0.04±0.01	0.70±0.03	2000-2012
Barcelona	1220	1.25±0.49	1.40±0.32	0.20±0.12	0.92±0.04	0.04±0.02	0.70±0.03	2005-2012
Burjassot	1045	1.27±0.45	1.28±0.33	0.18±0.12	0.93±0.03	0.03±0.02	0.70±0.03	2007-2013
Ersa	557	1.31±0.46	1.42±0.38	0.17±0.10	0.96±0.02	0.02±0.01	0.70±0.03	2008-2013
Ispra	1465	1.35±0.35	1.57±0.25	0.35±0.31	0.92±0.04	0.05±0.02	0.71±0.04	1997-2013
Lecce	1327	1.49±0.50	1.40±0.43	0.23±0.13	0.92±0.04	0.04±0.02	0.69±0.03	2003-2012
Messina	739	1.29±0.44	1.32±0.46	0.22±0.13	0.94±0.04	0.03±0.02	0.70±0.03	2005-2012
Modena	769	1.32±0.27	1.52±0.29	0.33±0.20	0.93±0.03	0.04±0.02	0.71±0.03	2002-2011
Moldova	1519	1.17±0.26	1.52±0.27	0.25±0.17	0.94±0.03	0.03±0.02	0.70±0.03	1999-2012
Potenza	608	1.33±0.72	1.35±0.41	0.17±0.11	0.92±0.05	0.04±0.03	0.70±0.03	2006-2012
Rome	1473	1.48±0.49	1.40±0.38	0.22±0.12	0.91±0.04	0.04±0.02	0.69±0.03	2001-2012
Thessaloniki	1042	1.28±0.26	1.56±0.31	0.30±0.16	0.94±0.03	0.03±0.01	0.70±0.03	2005-2012
Toulon	1008	1.27±0.44	1.49±0.30	0.17±0.11	0.93±0.03	0.03±0.01	0.69±0.03	2005-2010
Villefranche	975	0.98±0.36	1.50±0.33	0.20±0.14	0.95±0.03	0.03±0.01	0.71±0.03	2004-2012
Dust Affected Sites								
Blida	953	1.92±0.49	0.98±0.42	0.24±0.17	0.89±0.03	0.06±0.02	0.71±0.03	2004-2010
Malaga	869	1.57±0.47	1.06±0.37	0.17±0.11	0.90±0.03	0.05±0.02	0.71±0.02	2009-2012
Granada	1193	1.75±0.52	1.15±0.41	0.18±0.11	0.90±0.03	0.05±0.02	0.69±0.04	2005-2013
Forth Crete	1057	1.69±0.59	1.24±0.49	0.23±0.12	0.93±0.03	0.03±0.02	0.71±0.03	2003-2011
Lampedusa	789	2.17±0.67	0.95±0.50	0.20±0.14	0.92±0.03	0.04±0.02	0.71±0.03	2003-2012
Erdemli	1322	1.07±0.46	1.29±0.35	0.31±0.17	0.93±0.04	0.04±0.02	0.71±0.03	1999-2011
Sde Boker	3403	1.44±0.63	0.94±0.41	0.21±0.14	0.92±0.02	0.05±0.02	0.72±0.02	1996-2013
Nes Ziona	1264	1.37±0.62	1.05±0.43	0.28±0.16	0.91±0.06	0.05±0.04	0.72±0.04	2000-2012
Oristano	515	1.54±0.61	1.19±0.49	0.23±0.16	0.90±0.03	0.06±0.03	0.71±0.03	2000-2003

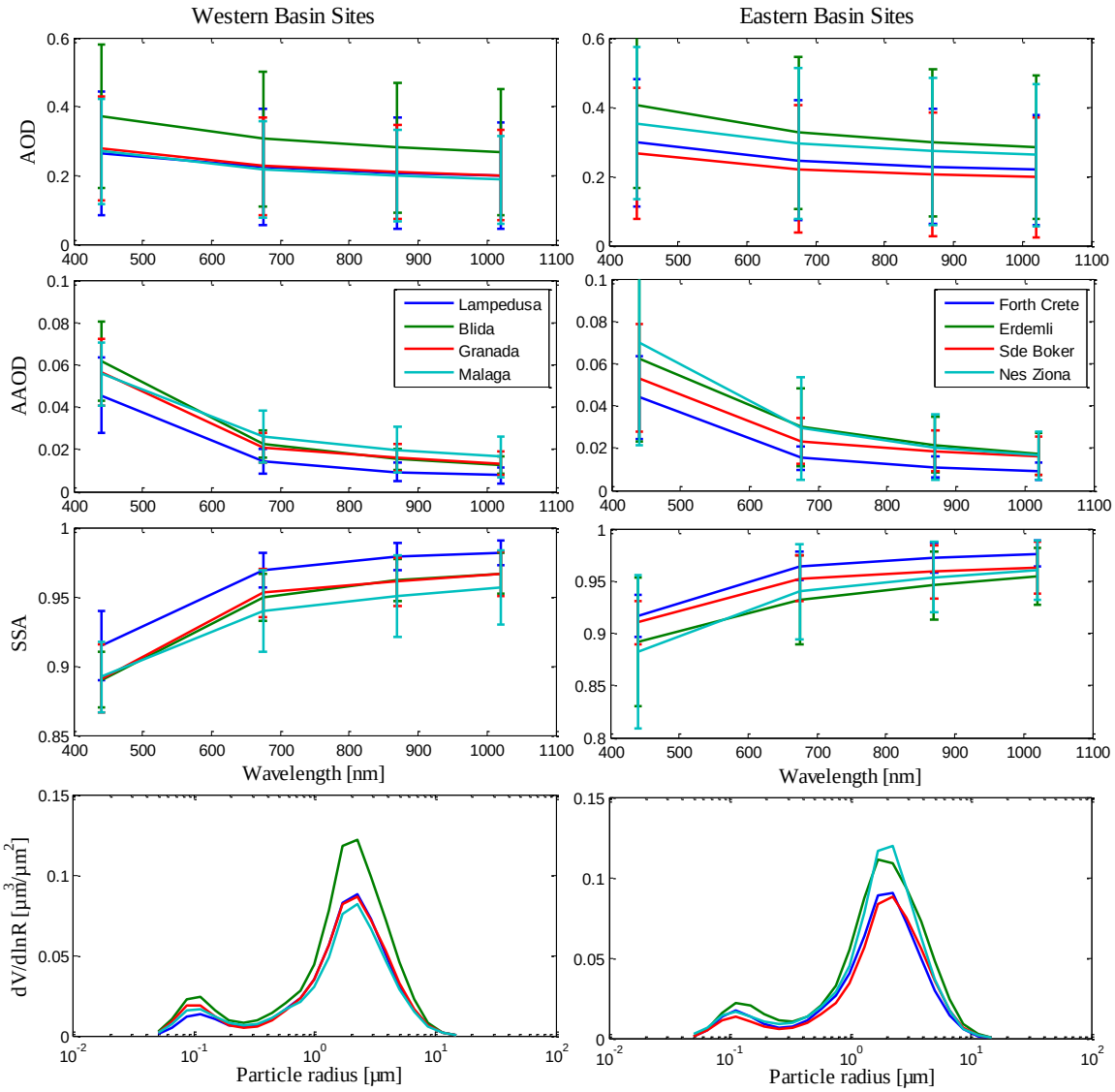

Fig. S1a The optical and microphysical properties of dust (EAE<0.6) aerosols for different dust affected sites in Mediterranean basin. The effect of sea salt could be seen in case of Lampedusa and Forth Crete in both SSA and AAOD spectral dependency. In spite of different plausible dust sources both eastern and western basin sites show a good consistency in optical and microphysical properties and could be regarded as dust model for the Mediterranean Basin.

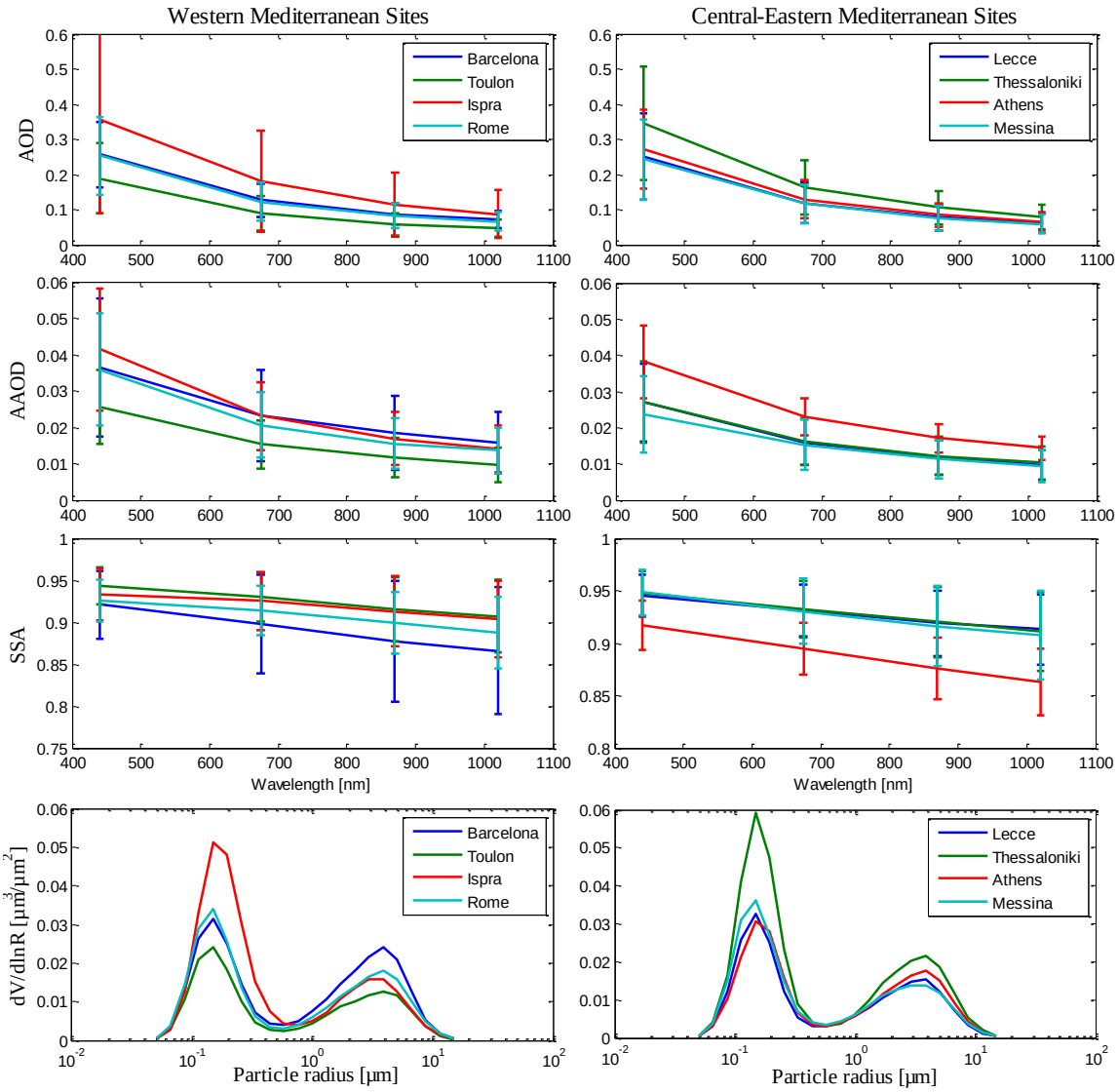

Fig. S1b Optical and microphysical properties of polluted continental (EAE>1.4) aerosols for different pollution dominated sites in Mediterranean Basin.

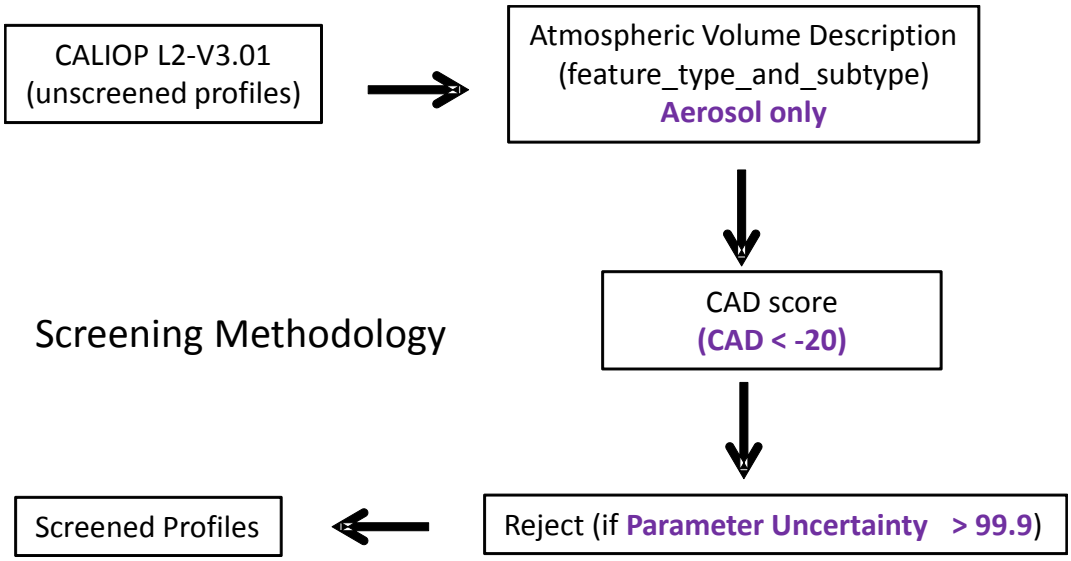

Fig. S2 Flow chart of screening methodology for CALIOP extinction profiles used in present study. The details can be found in Winker et al., 2013.

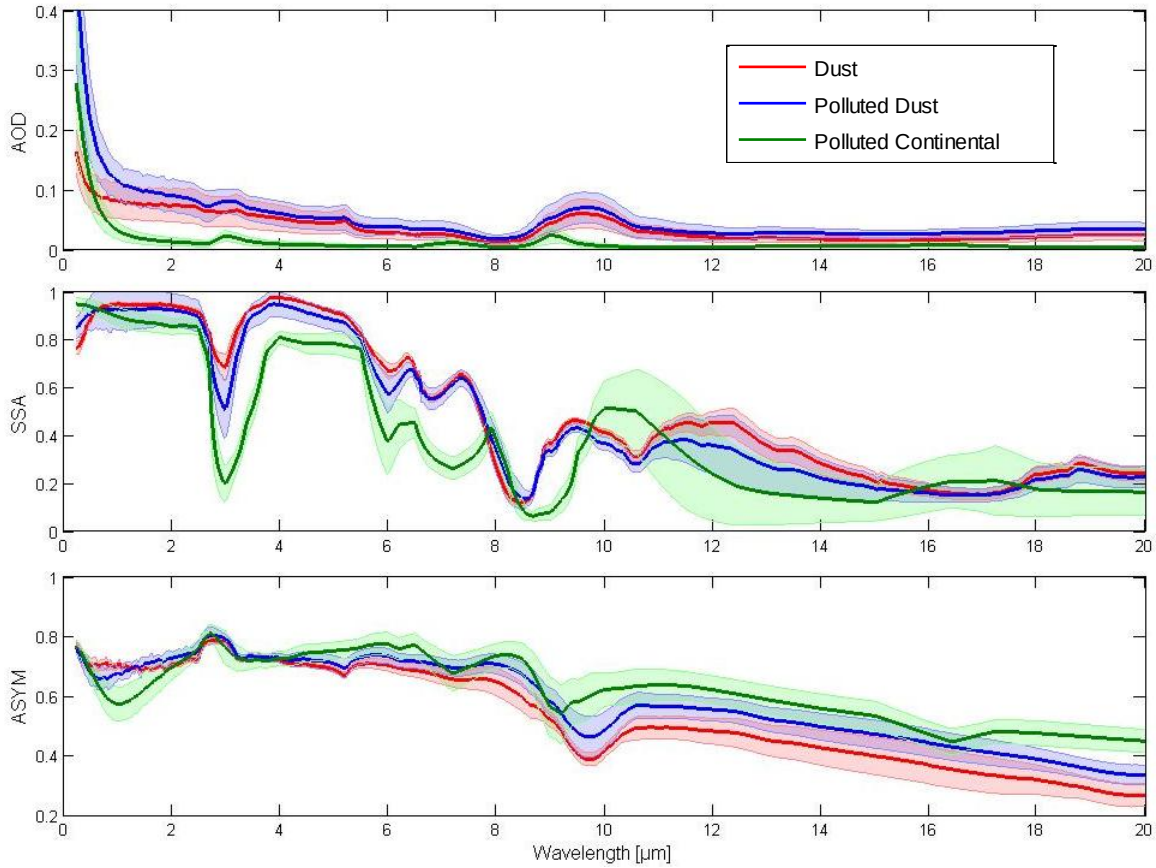

Fig. S3 AOD, SSA and ASYM for three different aerosol types in 0.25 – 20 µm wavelength region. The errors in calculation are shown by transparent shaded area. The methodology of calculation is given in main text (methodology section).

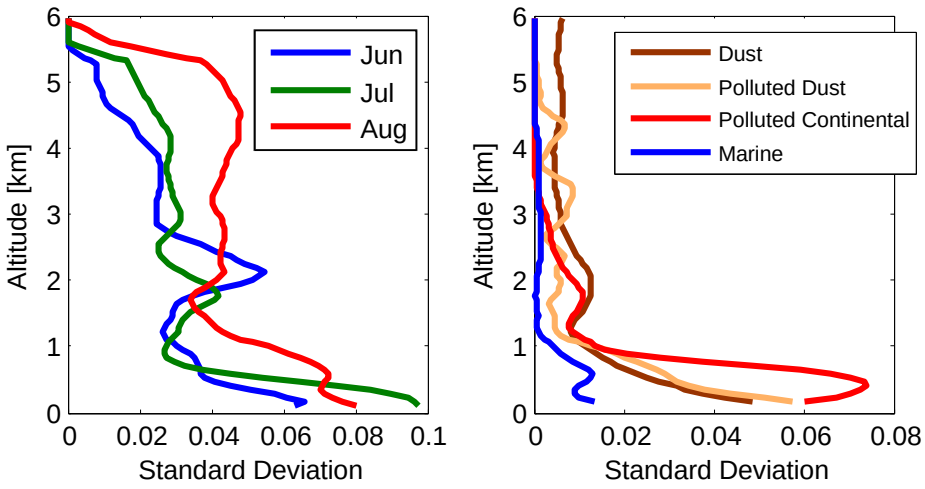

Fig. S4 Vertical distribution of standard deviation [km^{-1}] of monthly mean aerosol extinction coefficient (left panel) and seasonal mean (averaged from monthly mean) aerosol extinction coefficient for different dominant aerosols (right panel) during summer 2010. All points of individual profiles which did not characterized as aerosol (below<6 km altitude) are given 0.0 km^{-1} extinction values, which in results the higher standard deviation values.

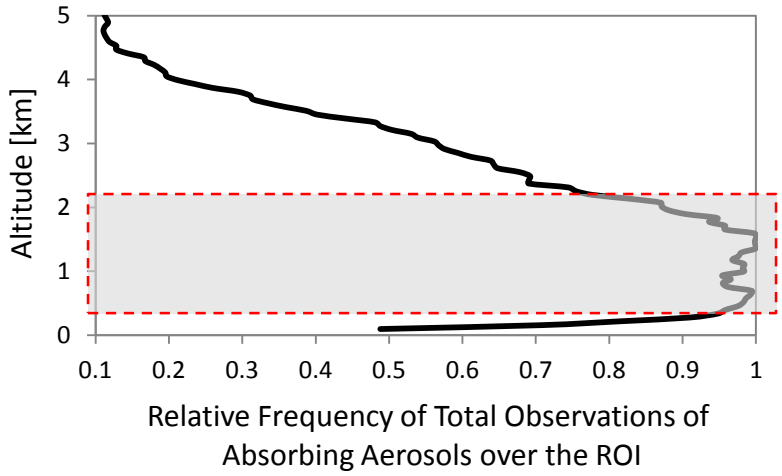

Fig. S5 CALIOP-derived relative frequency of total observations of absorbing aerosols over the ROI during summer 2010. This absorbing aerosols profile (averaged for dust, polluted dust and polluted continental aerosols types) is showing maximum number of aerosol layers resides between ~ 400-2200 m altitude ranges.

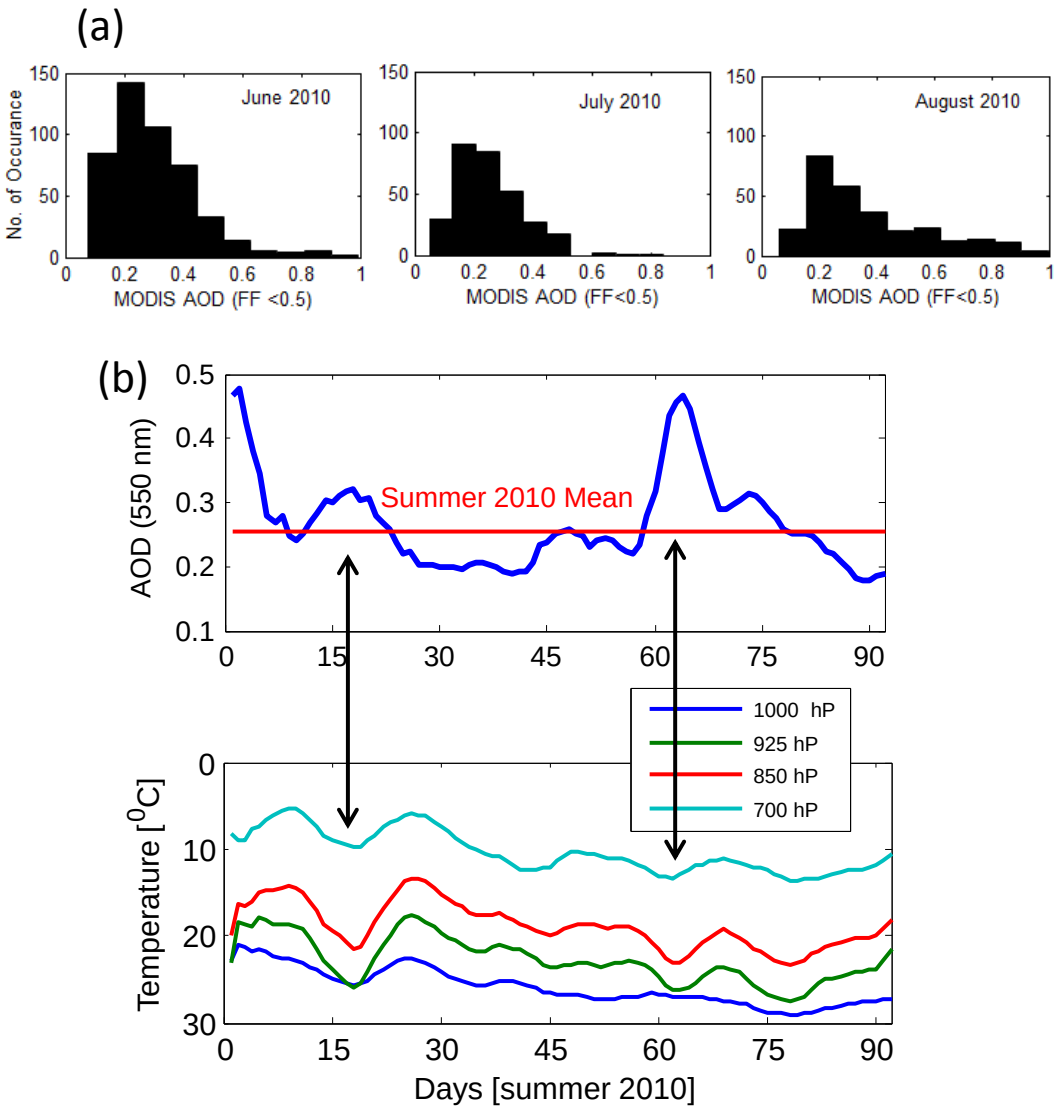

Fig. S6 (a) Occurrence frequency of MODIS AOD for *ff*<0.5 case during June – August, 2010, and (b) 7-day running mean of daily averaged AOD (upper panel) and atmospheric temperature at 4 pressure levels over the ROI.

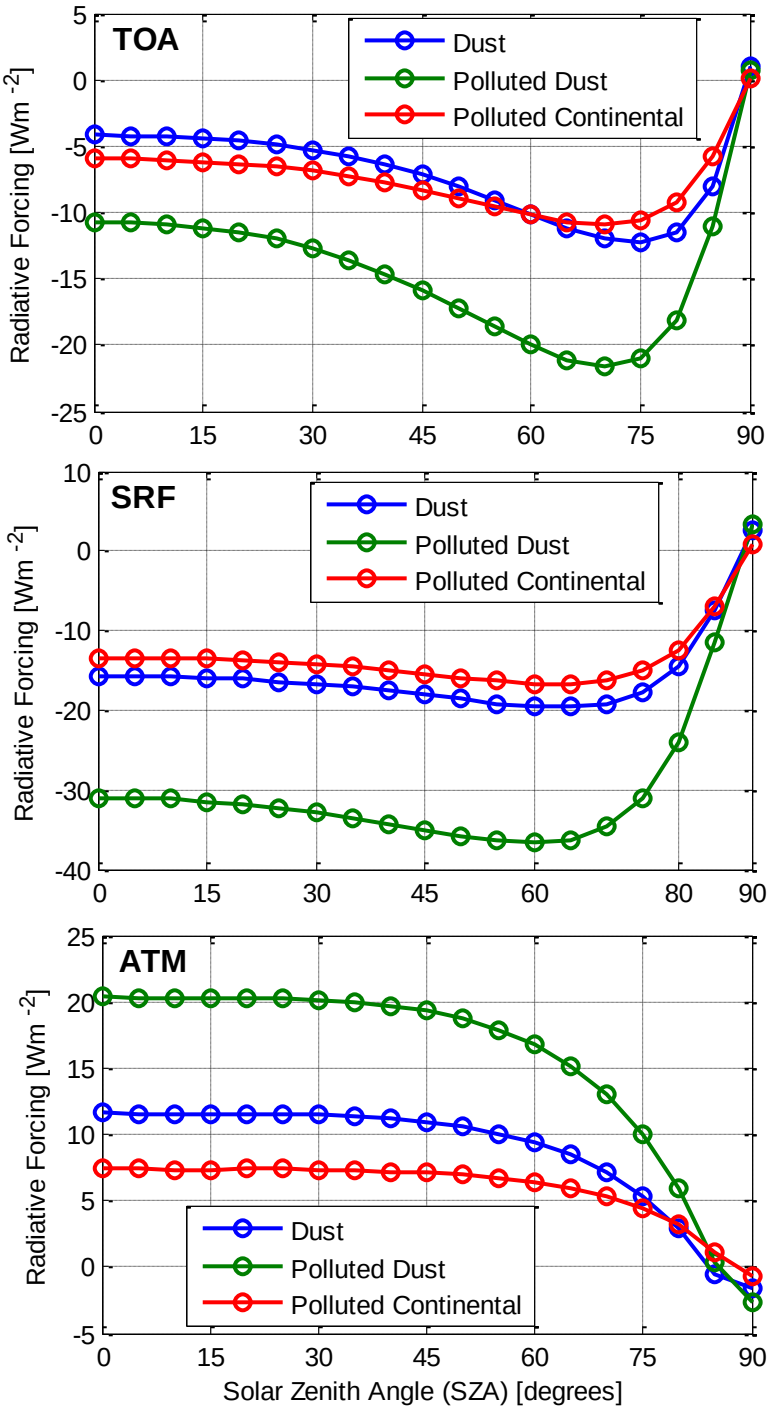

Fig. S7 Variation of radiative forcing of aerosol types (dust, polluted dust and polluted continental) with solar zenith angles (SZA) at TOA (upper panel), at SRF (middle panel) and in ATM (lower panel).

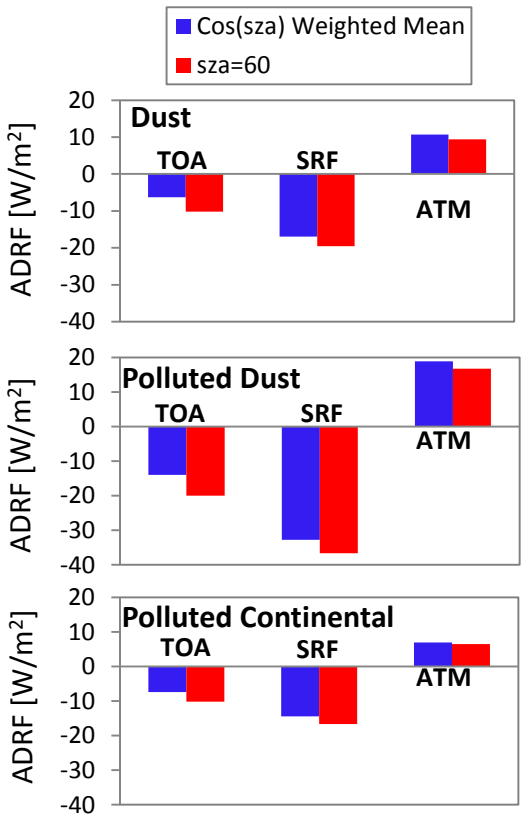

Fig. S8 Comparison of Aerosol Direct Radiative Forcing (ADRE) for sza=60^0 with Cos(sza) weighted mean for all three absorbing aerosols types at TOA, at SRF and in ATM.

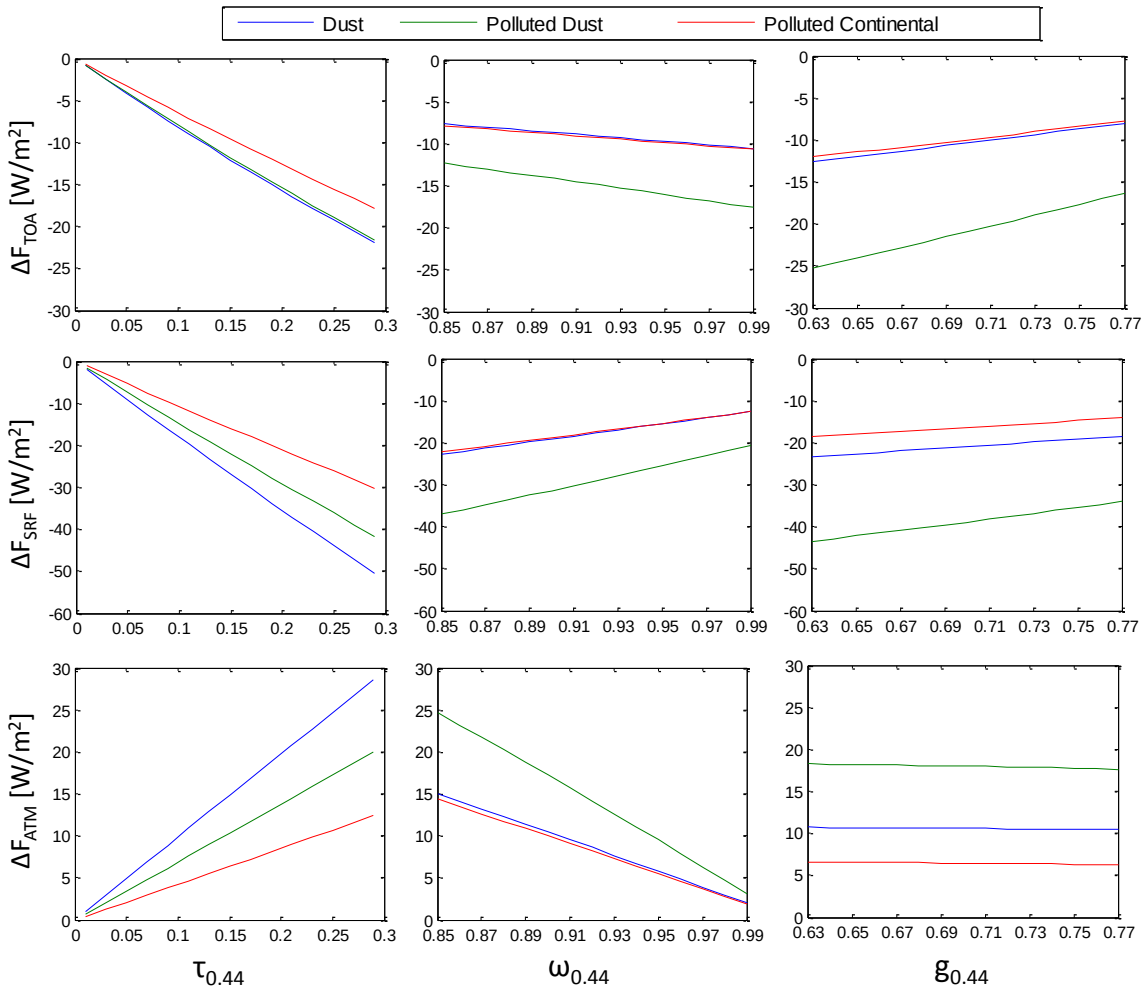

Fig. S9 Dependence of aerosol radiative forcing (integrated over the solar spectrum (0.25-20 µm and SZA = 60^0) on aerosol properties [AOD ($\tau_{0.44}$), SSA ($\omega_{0.44}$) and asymmetry parameter ($g_{0.44}$) at 0.44 µm] for different absorbing aerosols calculated from SBDART radiative transfer calculation. For each aerosol property the upper panel denotes forcing at top of the atmosphere (ΔF_{TOA}), middle one present forcing at surface (ΔF_{SRF}) and the lower one shows forcing in the atmosphere (ΔF_{ATM}).

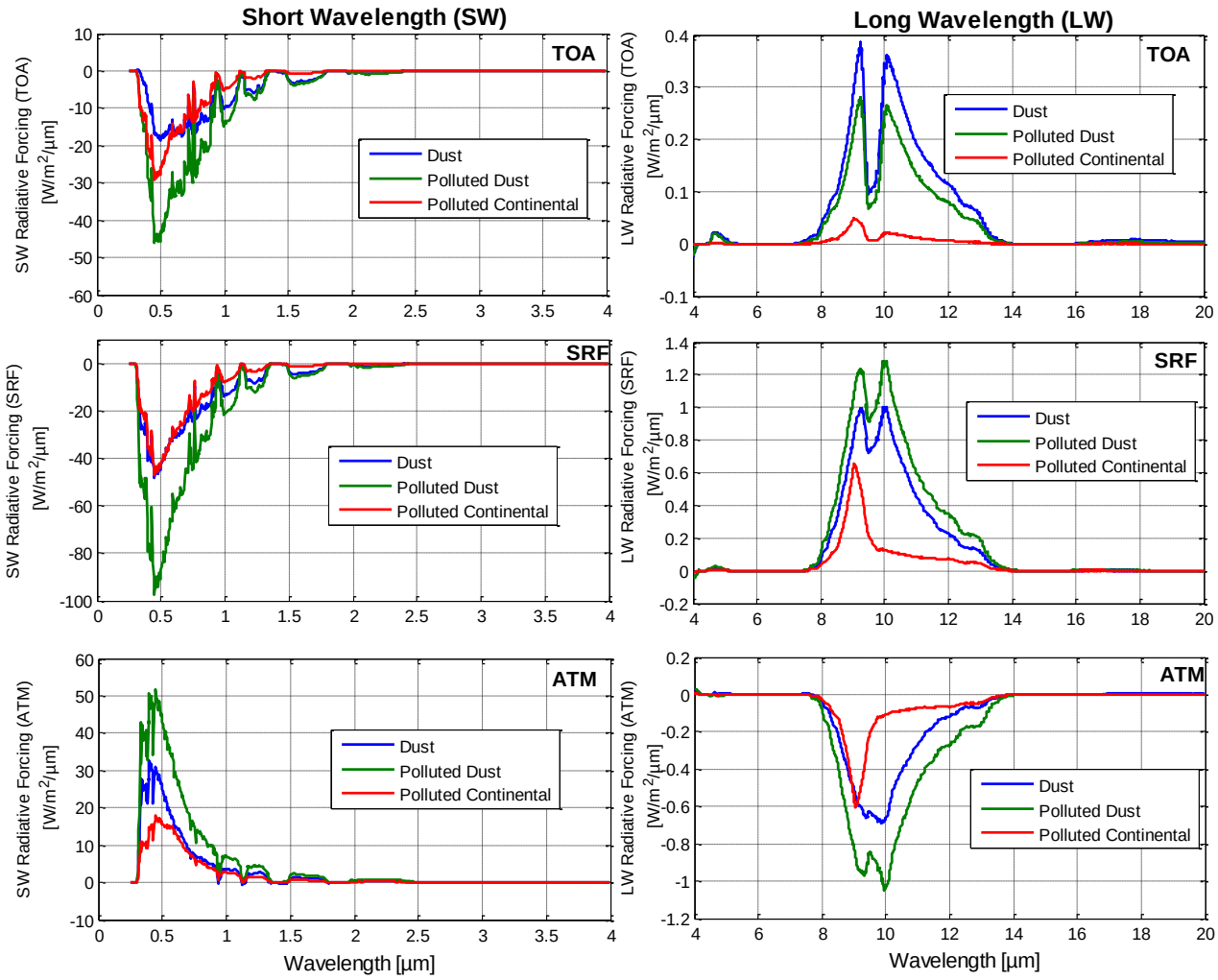

Fig. S10 Radiative forcing of different aerosol types as a function of wavelength in SW and LW region at TOA, SRF and in ATM.